Iranian Hydraulic Association
Journal of Hydraulics
Vol. 19, No. 4, PP. 69-78, Winter 2025

Research Article
https://doi.org/10.30482/jhyd.2024.407121.1712

Experimental and Numerical Study of Flow Over a Triangular (Crump) Weir with Variable Ramp Slopes Under Different Head Ratios

Fereshteh Sadat Mousavi Pour[1*]

1- University lecturer, Islamic Azad university of Qom, Civil Engineering Department, and PhD Candidate, Tehran University, Environment Department.

[*] **fereshte.mousavi@ut.ac.ir**

Received: 16 August 2024, Accepted: 16 December 2024 J. Hydraul. Homepage: www.jhyd.iha.ir

Abstract

To determine the free surface flow characteristics over a triangular broad crested (crump or hump) weir with different with different upstream and downstream slopes, a series of experiments were conducted in hydraulics laboratory using a 5 m long flume. The experiments were simulated by a numerical model, Flow-3D, in order to study the flow characteristics such as free surface elevation (water surface profile), Froude number, discharge coefficient and specially the location of critical flow state in different head ratios and ramp slopes. To investigate the hydrodynamic field over the weir, the computational results, included different turbulence models: two-equation k–ε, renormalized group (RNG), and large eddy simulation (LES). A nested mesh with higher resolution around the weir was employed and the computatinal results showed a close agreement with experimental data. Finally, according to the results it was found that when steeper ramp slope faces upstream, the critical flow occurs exactly at the crest of the weir, while milder ramp facing upstream makes the critical flow move backward just before the crest. The critical state location showed no sensetivity to different head ratios. Moreover, discharge coefficients were calculated and it is concluded that C_d equales 0.95 and 1.30 respectively for steep slope and mild slope facing upstream. It is worth mentioning that identification the accuracy of turbulence models' functionality among different ones offered by Flow-3D in such experiments, requires employing an additional criterion besides water surface elevation.

Keywords: critical flow location, fraud number, weirs, grade change, critical depth meters.

1. Introduction

Hydraulic structures such as weirs are used for flow measurement, water level and sediment control in water channels. There are a wide variety of weir designations which have been developed for various applications (Akbari et al., 2019). Furthermore, they are used as hydraulic jump control structure and compactness of stilling basins (Achour et al., 2022). In general, Weirs are categorized into sharp-crested and broad-crested groups. There are some proven advantages for each one. But broad-crested weirs are superior compared to other flow measuring structures, for instance: they show more stability rather than sharp-crested weirs, they are usually used as dams, especially in gabion weirs, etc., with sides ramps especially upstream face of the weir, they can easily pass sediments and floating objects (Malekzadeh et al., 2022). Triangular section or crump weirs can operate under partly submerged flow conditions while in addition it has the ability to transport sediments over the crest (Bos, 1976). Additional classifying methods are provided by researchers according to the weirs' geometry, function and flow condition. Broad and sharp crested weirs which were already mentioned are classified as geometry related group. Flow gauging, flood control and irrigation are counted as the function classifier while free or submerged state present flow condition (Al-Shukur et al., 2017). Several researches have been conducted in the past and recently to investigate weirs including simple and complex cross sections. Thus, useful empirical discharge equations have been proposed (Gogus et al., 2016). Equation 1 is the most common one used to compute the flow over the broad crested weir. Where Q, C_d, B, H and g are discharge (m^3/s), discharge coefficient, flume width (m), water head above the weir and gravity acceleration(m/s^2) respectively.

$$Q = C_d \frac{2}{3} B\sqrt{2g}H^{3/2} \quad (1)$$

For triangular section weirs Eq. 2 is proposed (Khalifa, 2021; Xu & Jin, 2017):

$$Q = C_d B\sqrt{g}H^{3/2} \quad (2)$$

The fixed relationship between flow depth and discharge that is the consequence of critical flow is the basis of considering this type of flow remarkable and also is the main reason for which weir structures are used widely.

$$y_c = \sqrt[3]{\frac{q^2}{g}} \quad (3)$$

Equation 2 determines the relation between q (m^2/s) and y_c (m) which stand for discharge and critical depth respectively. In case of flow meter weirs, different types of sections are introduced. Triangular broad crested ones, in particular, are known as leading the critical state occurrence at the grade change (Chaudhry, 2008). Bos (1989) conducted the first study of flow characteristics over a triangular broad-crested (crump or hump) weir with different ramp slopes in the upstream and downstream which is known as TW-UDR[1] from now on. He determined C_d under different head ratios and side slopes. A noticeable field of interest for researchers has been looking for a guidance leading to increase the discharge and also decrease the sedimentation before the weir (Zahabi et al., 2018). The effects of openings in the weir's body was studied in order to increase the flow rate (Daneshfaraz et al., 2021). A series of experiments was planned to study the effect of surface roughness and side slope of TW-UDR on the C_d. This plan concluded 18 TW-UDR models of different apex angles and three types of surface roughness. As one of the research's conclusions, it was demonstrated that the more surface roughness is increased, the greater reduction in C_d value is observed (Khalifa, 2021). Based on experimental analysis, past researchers have shown that discharge coefficient changes proportionally with h/L ratio (the ratio of water head above the weir to the length of the weir crest), maintaining an average range of C_d for various h/L values. A new concept to design of compound broad crested weir was proposed to measure wide range of discharges thereby maintaining a constant discharge coefficient irrespective of the head over weir (Kulkarni & Hinge, 2020). The numerical simulation of flow over a TW-UDR using the ANSYS Fluent software were repeated 437 times including the variation of side slopes, weir's height and discharge to clarify the impact on C_d. Then, multi-variable regression equations for estimating C_d were presented(Malekzadeh et al., 2022). The Flow-3D model together with laboratory model were

1 Triangular Weir with Upstream and Downstream Ramp

used to determine the free-surface profile of rectangular broad-crested weir and computational results agreement with experimental model was satisfying(Afshar & Hoseini, 2013). Flow-3D was used to calculate water flow profile over a rectangular broad-crest weir and in Gharnave check dam in north east of Iran. According to simulation outputs, the performance of this software in prediction of flow profile and hydraulic jump is reliable (Maghrebi et al., 2012). Efforts were made to study the influence of geometric parameters on flow regime by means of Flow-3D in a comparing straight weir and rectangular labyrinth weir. The computational model was validated by measured surface profiles and velocities in laboratory (Mirkhorli et al., 2024). The word" weir" will be used to describe any structure used to determine the volume of flow of water from measurements of its depth on a crest or sill of known length and form (Horton, 1907). comparing one-equation, k-ε, RNG k-ε, and k-ω turbulence models for simulating the full free surface profile of flow over a floodway from upstream to downstream showed no noticeable difference in the accuracy of estimation (Helmi, 2019). According to the reviewed studies, it is common to formulate and calculate C_d under the consideration of critical state on the crest of the weirs. Thus, in this paper the main goal is to answer whether it is true or not in case of triangular broad section weirs. Additionally, experimental free surface profile and Q data were validated using Flow-3D.

2. Methodology

2.1. Experimental setup

To determine the free surface flow characteristics over a TW-UDR, two sets of experiments were conducted in a hydraulic laboratory using a rectangular section flume. The flume was 5 m long, 0.081 m wide and 0.15 m deep with glassed bed and walls. A TW-UDR was placed 2 m away from the flow entrance of the flume. The scheme of physical model is shown in Fig. 1(c). The TW-UDR weir included two sides sloped about 28 and 72 degrees, height and length of 42 and 194 mm respectively. The weir was made of smooth material that the impact of friction is negligible. Head ratio was measured using a hydraulics bench connected to the flume so that they make a closed-circuit system equipped with a pump-controlled hydraulic system which delivers the flow rates. It provides an accurate discharge adjustment (Kheiralla et al., 2007). Both upstream entrance and downstream end of the flume were connected to a stilling basin of water supplying a smooth and uniform flow (Imanian et al., 2021). For the sake of accuracy, the speed of water discharge was measured in three levels to determine the flow rate in each stage of the experiment. The flume was divided into different long and short distances from upstream to downstream on the basis of variations in the water surface profile. The water surface elevation was measured at these specific marked distances by means of a needle-pointed plumb bob attached to a graduated steel tape moving along the flume with the least count of 1 mm.

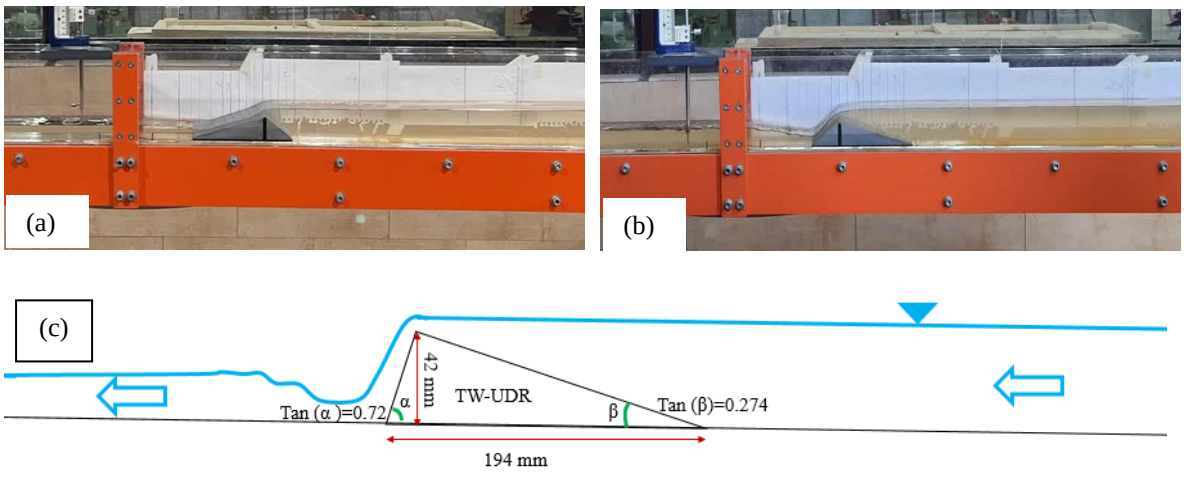

Fig. 1 (a) View of the laboratory flume and the weir block used in the first experiment set, (b) second experiment set and (c) schematic of the physical model.

In the first set of the experiment, steeper ramp of the weir faced upstream (Fig. 1a) and in 9 different head ratios (measured by hydraulics bench), the free surface elevation was measured at 17 specific marked locations along the flume.

Milder ramp was faced upstream in the second set (Fig. 1b) and the procedure was repeated. Fig. 2 shows the measuring locations in details.

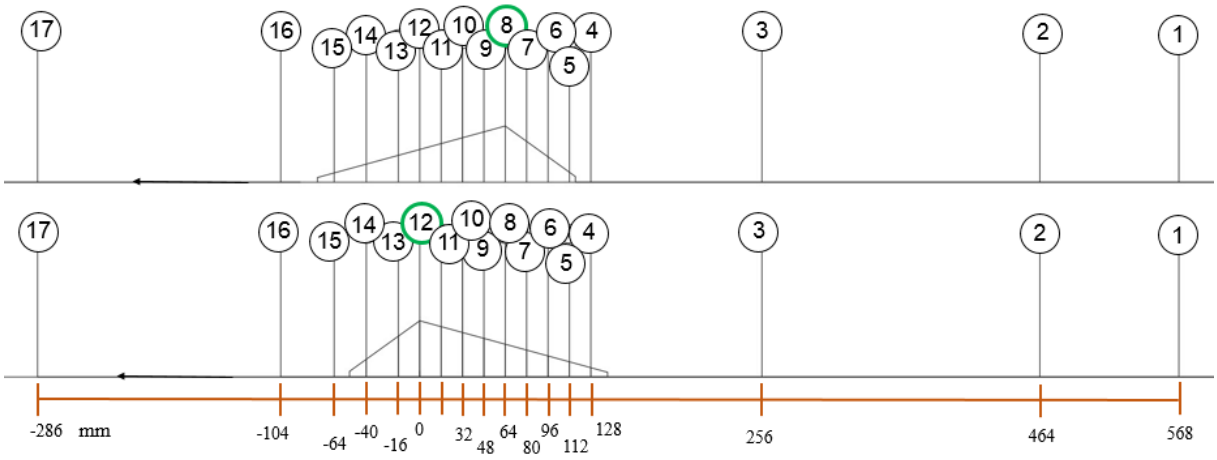

Fig. 2 Free surface elevation measuring locations (marked points).

2.2. Numerical setup

2.2.1. Numerical model

In this study Flow-3D, a commercial CFD model developed by Flow Science in Santa Fe New Mexico (Rady, 2011), was hired to simulate the flow characteristics over the weir. Flow-3D applies numerical methods to solve the Navier-Stokes equations which are the base of the software. This software uses finite volume method (FVM) and as this method needs small usage of memory, it gives solutions faster even for complex problems(Ayoob & Hamad, 2022). The momentum and continuity equations used by the software to solve the PDEs[1] are as shown in Eqs. 3 and 4 where R_{SOR}, ρ, V_f, A_z, A_y and A_x represent the mass source, mass density of fluid, fractional volume and area open to flow respectively. U, v and w stand for the velocity components in x, y, and z directions while c^2 and p demonstrate square of the sound and pressure. R and ξ are coordinates-dependent coefficients which are set to unity for cartesian coordinates (Hilo et al., 2018; Hilo et al., 2021; Kumar & Raj, 2022).

$$\frac{\partial w}{\partial t}+\frac{1}{V_f}\{uA_x\frac{\partial w}{\partial t}+vA_yR\frac{\partial w}{\partial y}+wA_zR\frac{\partial w}{\partial z}\} \quad (4)$$
$$=-\frac{1}{\rho}\frac{\partial P}{\partial z}+G_z+f_z+b_z-\frac{R_{SOR}}{\rho V_f}(W-W_w-\partial W_S)$$

$$\frac{V_f}{\rho c^2}\frac{\partial}{\partial t}+(uA_x)+R\frac{\partial}{\partial y}(vA_y)+\frac{\partial}{\partial z}(wA_z)+$$
$$\xi\frac{uA_x}{x}=\frac{R_{SOR}}{\rho} \quad (5)$$

Flow-3D provides Prandtl's mixing length , k^2, standard k – ε, k –ε RNG, k-ω two-equation and LES turbulence models (Man et al., 2019). Selecting a correct turbulence model which results in a closed form of the Navier–Stokes equations is highly recommended (Afshar & Hoseini, 2013). In this study according to the software's user manual recommendation k–ε, RNG and the LES turbulence models were tested. The RNG is the developed form of two-equation k−ε model during many years later (Yakhot & Smith, 1992). The base of Reynold's stress observation comparably as the viscous stress is k−ε model. According to Boussinesq approximation, the turbulence eddy viscosity (υ_t) is the solution key of the turbulence equation (Eq.6).

$$\upsilon_t=C_\mu\frac{k^2}{\varepsilon} \quad (6)$$

C_μ, k and ε are an empirical coefficient, turbulence kinetic energy and dissipation, respectively(Hami, 2021).

1 Partial Differential Equations

2 one equation turbulent energy

In the standard k–ε turbulence method, both k and ε are extracted from Equations 7 and 8 which are as follows:

$$\frac{\partial k}{\partial t}+u_i\frac{\partial k}{\partial x_i}=\frac{\partial}{\partial x_i}(\frac{\upsilon_t}{\partial k}\frac{\partial k}{\partial x_i})+\upsilon_t(\frac{\partial u_i}{\partial x_j}+\frac{\partial u_j}{\partial x_i})\frac{\partial u_i}{\partial x_j}-\varepsilon \quad (7)$$

$$\frac{\partial \varepsilon}{\partial t}+u_i\frac{\partial k}{\partial x_i}=\frac{\partial}{\partial x_i}(\frac{\upsilon_t}{\partial_\varepsilon}\frac{\partial \varepsilon}{\partial x_i})+C_1\frac{\varepsilon}{k}\upsilon_t \quad (8)$$
$$(\frac{\partial u_i}{\partial x_j}+\frac{\partial u_j}{\partial x_i})\frac{\partial u_i}{\partial x_j}-C_2\frac{\varepsilon^2}{k}$$

C1, C2 are considered constant and equal to 1.44 and 1.92 to adjust the generation and dissipation of turbulence in ε equation. σ_k and σ_ε are 1.0 and 1.3.
LES kinematic eddy viscosity (υ_T) is determined by equation 9:

$$\upsilon_T=(cL)^2\sqrt{2e_{ij}2e_{ij}} \quad (9)$$

In the above equation, c is constant and equal to 0.1 - 0.2 while L and e_{ij} are length scale and strain rate tensor components (Man et al., 2019).

2.2.2. Mesh and Geometry

The TW-UDR weir was plotted by AutoCAD 3D, then exported to Flow-3D as lithography format (*.stl). An inner remove domain of solid weir was defined to be neglected in simulation procedure. Moreover, to decrease the simulation time according to symmetry in y direction, only half of the physical model was considered in Flow-3D.
To provide outputs with high accuracy, suitable size and number of cells should be defined. Fractional area/volume method [1] allows a rectangular computational cell to be partially blocked by an obstacle(Liu & García, 2008).
Applying a uniform mesh to the whole domain is computationally very expensive, so discretization was performed with a high resolution around the weir. For mesh sensitivity analysis the developed model was performed with three grid sizes of 4, 3 and 2 mm in general and nested (higher resolution) mesh around the weir of 2, 1.5 and 1 mm respectively. The calculated Q, water surface elevation and weir shape for three sets of grid sizes were compared with observed data. Using the grid size from 3 and 1.5 to 2 and 1 confirmed that the results are still sensitive to grid size while decreasing the mesh size to 1 and 0.5 did not show any variations and led to independent results. Considering cost and time reduction, finally, the grid size of 2 and 1 mm was selected as rational a choice. Fig. 3 depicts the mesh and geometry used in numerical model.

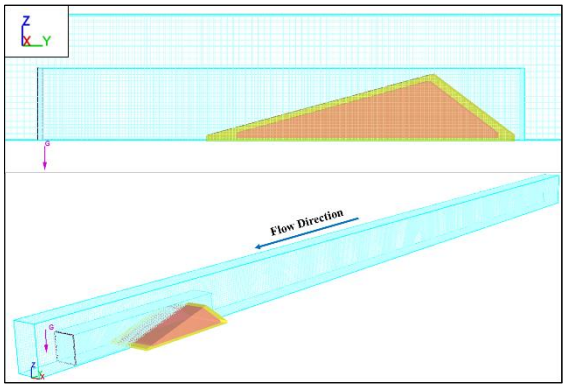

Fig. 3. Course and fine (nested) mesh blocks, removal domain and half of the physical model.

2.2.3. Boundary and Initial Conditions

The dominant fluid flow PDEs solutions extracted from boundary and initial conditions are highly governing the results. Six boundary conditions illustrated in Fig. 4 are as follows:

1. Course mesh block:
Y-max. and min. (weir's upstream and downstream): Specified pressure (P).
X-max. and min. (flume sides): Wall (W). Z-max. (water surface): Symmetry (S).
Z-min. (flume's bottom): Wall (W).

2. Fine mesh block:
Y-max. and min. (weir's upstream and downstream): Symmetry (S).
X-max. and min. (water surface): Symmetry (S).
Z-max. (Water surface): Symmetry (S).
Z-min. (flume's bottom): Wall (W).

Since hydraulic jump was observed in the downstream of the weir, in order to make it happen in the numerical model, a specified pressure as fluid elevation at the 17th measuring location (outlet) equal to observed water elevation in the laboratory was applied.

1 FAVOR

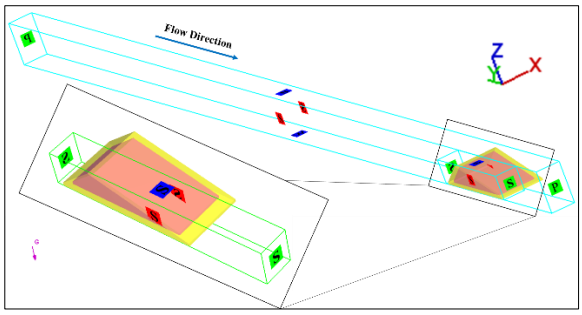

Fig. 4 Boundary conditions of the numerical model.

2.2.4. Fluid Characteristics and Physics

Here, the mass density of the water, dynamic viscosity, temperature and gravity in Z direction were set to 1gm/cm^3, 0.01gm/cm.sec, 20°C and -980 cm/sec^2 besides activation viscous flow.

3. Results and discussion

Two 9-stage sets of experiment were conducted consisted of 918 water depth measuring points and 18 different head ratios. It is worth mentioning each stage was repeated three times in order to minimize the errors. C_d and y_c were calculated by means of equation 2 and 3 while discharge was obtained from hydraulics bench directly. Marked points were selected and fixed according to critical flow appearance after several trial and errors. The comparison of every point's elevation with y_c and extracting its fraud number led to find the location of critical flow.

3.1. Free surface validation

Enabling two equation k–ε, RNG and LES turbulence models in Flow-3D, the water surface elevations under different head ratios were measured at marked points. Tables 1 and 2 present the comparison of experimental free surface profiles and calculated ones using RMSE[1] and MAE[2] indicators in equations 10 and 11 (Hodson, 2022).

$$RMSE = \sqrt{\frac{1}{N}\sum_{i=1}^{n}(y_{\exp} - y_{calc})^2} \quad (10)$$

$$MAE = \frac{1}{N}\sum_{i=1}^{n}\left|y_{\exp} - y_{calc}\right| \quad (11)$$

Where y_{exp} and y_{calc} are the experimental and calculated elevations.

As one can observe in Fig. 5, in both sets of experiments (a) and (b), the simulated free surface profile computed by three turbulence models under several discharges showed no significant difference. To be more precise, on one hand, while the results of RMSE equation for k–ε and LES are almost equal, RNG model

Table 1 Error analysis of the calculated free surface profile and observed data in experiment set (a).

Marked point number	Turbulence model	RMSE	MAE	Marked point number	Turbulence model	RMSE	MAE
	k–ε	0.0005	0.0005		**k–ε**	0.0040	0.0039
2	**RNG**	0.0004	0.0003	9	**RNG**	0.0042	0.0037
	LES	0.0004	0.0003		**LES**	0.0040	0.0033
	k–ε	0.0010	0.0009		**k–ε**	0.0028	0.0027
3	**RNG**	0.0010	0.0008	10	**RNG**	0.0031	0.0030
	LES	0.0010	0.0008		**LES**	0.0031	0.0030
	k–ε	0.0019	0.0016		**k–ε**	0.0022	0.0022
5	**RNG**	0.0021	0.0017	11	**RNG**	0.0023	0.0023
	LES	0.0021	0.0017		**LES**	0.0023	0.0023
	k–ε	0.0019	0.0016		**k–ε**	0.0017	0.0016
6	**RNG**	0.0015	0.0013	12	**RNG**	0.0024	0.0024
	LES	0.0015	0.0013		**LES**	0.0024	0.0024
	k–ε	0.0013	0.0010		**k–ε**	0.0028	0.0028
7	**RNG**	0.0014	0.0011	13	**RNG**	0.0030	0.0030
	LES	0.0014	0.0011		**LES**	0.0030	0.0030
	k–ε	0.0011	0.0009		**k–ε**	0.0013	0.0013
8	**RNG**	0.0011	0.0009	14	**RNG**	0.0021	0.0020
	LES	0.0011	0.0009		**LES**	0.0016	0.0016

1 Root-Mean-Squared Error.

2 Mean Absolute Error.

Table 2 Error analysis of the calculated free surface profile and observed data in experiment set (b).

Marked point number	Turbulence model	RMSE	MAE	Marked point number	Turbulence model	RMSE	MAE
	k–ε	0.0016	0.0012		**k–ε**	0.0015	0.0014
2	**RNG**	0.4060	0.0012	9	**RNG**	0.0095	0.0014
	LES	0.0016	0.0012		**LES**	0.0015	0.0014
	k–ε	0.0012	0.0012		**k–ε**	0.0010	0.001
3	**RNG**	0.1981	0.0012	10	**RNG**	0.0243	0.001
	LES	0.0012	0.0012		**LES**	0.0010	0.001
	k–ε	0.0023	0.0017		**k–ε**	0.0009	0.0007
5	**RNG**	0.0542	0.0017	11	**RNG**	0.0394	0.0007
	LES	0.0023	0.0017		**LES**	0.0009	0.0007
	k–ε	0.0024	0.0022		**k–ε**	0.0013	0.0011
6	**RNG**	0.0384	0.0022	12	**RNG**	0.0514	0.0015
	LES	0.0024	0.0022		**LES**	0.0015	0.0015
	k–ε	0.0018	0.0017		**k–ε**	0.0021	0.0018
7	**RNG**	0.0234	0.0017	13	**RNG**	0.0553	0.0018
	LES	0.0018	0.0017		**LES**	0.0020	0.0014
	k–ε	0.0020	0.0018		**k–ε**	0.0016	0.0016
8	**RNG**	0.0087	0.0018	14	**RNG**	0.0601	0.0012
	LES	0.0025	0.0022		**LES**	0.0012	0.0012

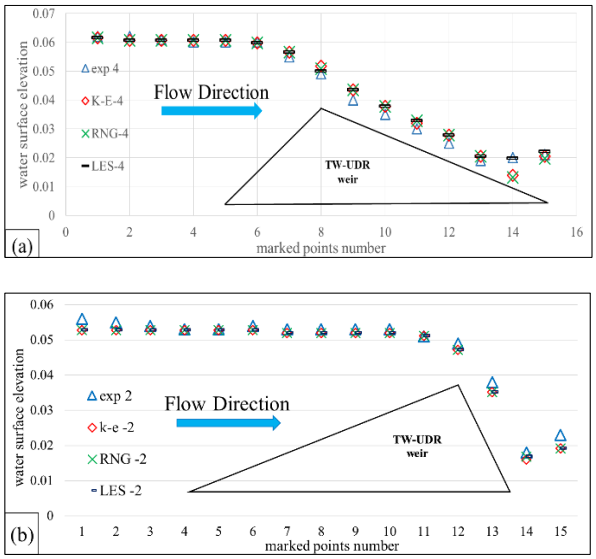

Fig. 5 Free surface profiles computed by different turbulence models in the second stage of experiment sets (a) and (b).

consequences are different. On the other hand, MAE equation leads to completely the same errors in three models. Additionally, the computed profiles are in rationale agreement with experimental data. Thus, it is clear that an extra criterion but water surface elevation is required to be employed to identify the accuracy of turbulence models' functionality in such experiments.

3.2. Critical flow

The main propose of this study was to identify the exact location in which critical flow appears. In order to achieve this goal, the marked points were placed in close distances just around the grade change of the weir in both sets of experiment as it is shown in Fig. 2. It was supposed that the critical state happens at the crest of the weir in agreement with past researches. In the first set of experiment, the steeper ramp facing upstream, the fact was proven again. To explain in more details, the subcritical flow ($y < y_c$) decreasing its depth reaches to critical state hitting the grade change exactly at the crest of the weir where y equals to y_c. Then, water depth drops more rapidly, so that fraud number exceeds one and the flow turns into supercritical state. Passing the weir, a hydraulic jump occurs and again flow state turns into subcritical. But in the second set, the milder ramp facing upstream, while the subcritical flow moves upward, the water depth declines gradually until it equals to y_c before (between points number 11 and 12) the grade change. Water passes the crest in a supercritical state with a y less than y_c. Finally, the water depth drops immediately along the steep ramp till the hydraulic jump occurs. It is worth to mention that under different nine head ratios the observed location of critical state stayed

constant as it is represented in table 3. The critical depths are obtained from the equation 3.

3.3. Coefficient of discharge

Under several various head ratios, the C_d was derived from the equation 2 in both sets of the experiment and according to Fig. 6, it is understood that the changes in the C_d number VS discharge shows no upward or downward tendency as it follows a horizontal trendline. C_d equals to 0.95 and 1.30 for steeper and milder slope facing upstream respectively. Further, comparing two sets of experiment confirms that locating the mild slope toward the stream flow results in an increase of 0.35 in the coefficient of discharge.

Table. 3 Water depths at the grade change (point 8) in experiment set (a) and at points 11 and 12 in experiment set (b).

Experiment set	q_{exp} (m^2/s)	y_c (m)	$y_{point\ 8}$ (m)
a	0.002408	0.008394	0.009
	0.004889	0.013458	0.014
	0.004029	0.011829	0.012
	0.004522	0.012776	0.013
	0.005176	0.01398	0.015
	0.006282	0.015906	0.017
	0.006747	0.016681	0.018
	0.010128	0.021869	0.023
	0.013128	0.025999	0.027

Experiment set	q_{exp} (m^2/s)	y_c (m)	$y_{point\ 11}$ (m)	$y_{point\ 12}$ (m)
b	0.001889	0.007139	0.0124	0.006
	0.002297	0.008133	0.0134	0.007
	0.003553	0.010878	0.0164	0.009
	0.005237	0.014089	0.0204	0.012
	0.006636	0.016498	0.0214	0.014
	0.00759	0.018043	0.0234	0.015
	0.009019	0.020242	0.0264	0.017
	0.012284	0.024873	0.0294	0.021
	0.014094	0.027259	0.0314	0.023

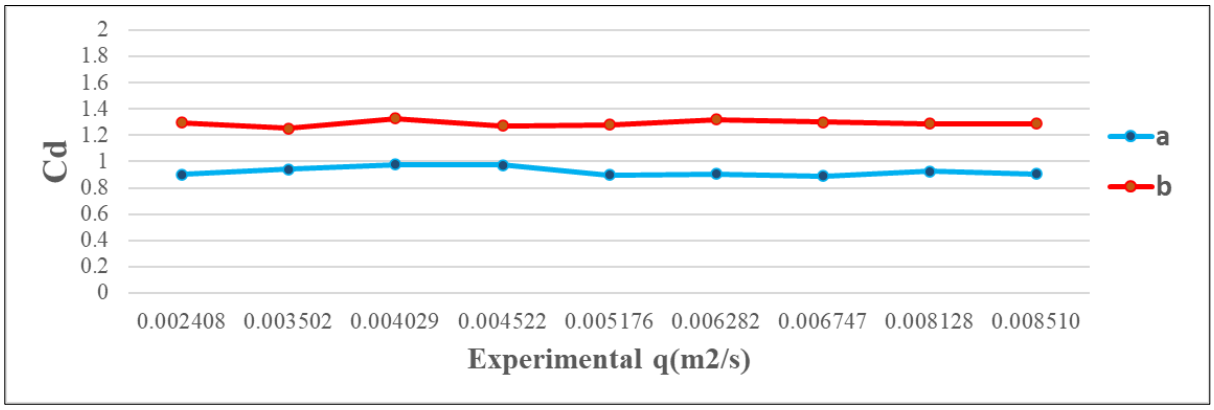

Fig. 6 Discharge coefficients under different head ratios in experiment sets (a) and (b).

4. Conclusions

In this research, the flow over a triangular-section weir (TW-UDR) with two different ramp slopes was investigated simultaneously through experimental and numerical approaches. The experiment consisted of two sets. Set (a) refers to a steeper ramp facing upstream, while in set (b), the weir was rotated 180 degrees. The experimental part was conducted in a laboratory using a flume connected to a hydraulics bench to observe the flow characteristics over the weir. To demonstrate the accuracy of the measured data, a CFD model was employed. Using Flow-3D, the numerical model, the experiment was simulated. The computed results obtained from the numerical simulation using three turbulence models (standard k–ε, RNG and LES) were compared with the experimental observations obtained from the physical model. The main outcomes of the undertaken efforts to study the flow characteristics under different head ratios are summarized as follows:

1. The computed free surface profile using three different turbulence models in sets (a) and (b) sets of experiment under various discharges showed no significant difference. All of results were in reasonable agreement with the measured data. Therefore, an extra criterion apart from water surface elevation such as velocity is required to determine the superiority of the turbulence models in simulating the most accurate answers.
2. A comparison of measured water depth and critical depth determined that the critical state occurs exactly at the grade change (point 8) in experiment set (a) when the steeper ramp faces upstream. However, in set (b), it appears before the

weir's crest (between points 11 and 12). In fact, this outcome was the main goal of the conducted study. It is worth mentioning that, in structural design the assumption of occurring the critical state at the weir's crest is commonly employed.

3. The location of the critical state did not show noticeable sensitivity to head ratio alterations. The separation zone was not observed during the experiment and the same result was reflected in the numerical analysis.

The discharge coefficients were calculated for both experimental sets. They were equal to 0.95 and 1.30, respectively, in sets (a) and (b).

6. References

Achour, B., Amara, L., Mehta, D. & Balaganesan, P. (2022). Compactness of Hydraulic Jump Rectangular Stilling Basins Using a Broad-Crested Sill. *LARHYSS Journal, 51*, 31-41.

Afshar, H. & Hoseini, S.H. (2013). Experimental and 3-D numerical simulation of flow over a rectangular broad-crested weir. *International Journal of Engineering and Advanced Technology*, *2*(6), 214-219.

Akbari, M., Salmasi, F., Arvanaghi, H., Karbasi, M. & Farsadizadeh, D. (2019). Application of Gaussian process regression model to predict discharge coefficient of Gated Piano Key Weir. *Water Resources Management, 33*, 3929-3947.

Al-Shukur, A., Al-jumaily, M. & Shaker, Z. (2017). Experimental investigation of flow characteristics over crump weir with Different conditions. *Saudi Journal of Engineering and Technology*, *2*(10), 373-379.

Ayoob, N.S. & Hamad, A.M. (2022). Numerical simulation for flow over a broad-crested weir using FLOW-3D program. *Civil Engineering and Architecture*, *10*(5), 2157-2171.

Bos, M.G. (1976). Discharge measurement structures. International Institute for Land Reclamation and Improvement/ILRI, Wageningen, The Netherlands.

Chaudhry, M.H. (2008). Open-channel flow, 2nd Ed., Springer.

Daneshfaraz, R., Minaei, O., Abraham, J., Dadashi, S. & Ghaderi, A. (2021). 3-D numerical simulation of water flow over a broad-crested weir with openings. *ISH Journal of Hydraulic Engineering*, *27*(sup1), 88-96.

Gogus, M., Al-Khatib, I.A., Atalay, A.E. & Khatib, J.I. (2016). Discharge prediction in flow measurement flumes with different downstream transition slopes. *Flow measurement and Instrumentation*, *47*, 28-34.

Hami, K. (2021). Turbulence Modeling a Review for Different Used Methods. *International Journal of Heat & Technology*, *39*(1), 227-234.

Helmi, A.M. (2019). Assessment of CFD turbulence models for free surface flow simulation and 1-D modelling for water level calculations over a broad-crested weir oodway. *Water SA*, *45*(3), 420-433.

Hilo, A.N., Abid, S.R. & Daek, Y.H. (2018). Numerical model for flow on stilling basin type III. 2018 International Conference on Advance of Sustainable Engineering and its Application (ICASEA),

Hilo, A.N., Ayoob, N.S. & Daek, Y.H. (2021). Numerical simulation to evaluate the effect of the stepped chute on abrasion erosion of a stilling basin type III. IOP Conference Series: Materials Science and Engineering,

Hodson, T.O. (2022). Root mean square error (RMSE) or mean absolute error (MAE): When to use them or not. *Geoscientific Model Development*, *15(14)*, 5481-5487.

Horton, R.E. (1907). Weir experiments, coefficients, and formulas (revision of Water-Supply Paper 150), Department of the Interior, United States Geological Survey, Washington.

Imanian, H., Mohammadian, A. & Hoshyar, P. (2021). Experimental and numerical study of flow over a broad-crested weir under different hydraulic head ratios. *Flow measurement and Instrumentation*, *80*, 102004, https://doi.org/10.1016/j.flowmeasinst.2021.102004.

Khalifa, S.Y. (2021). Effect of Height Variation on Coefficient of Discharge for Crump Weir. *ATBU Journal of Science, Technology and Education*, *9*(1), 22-37.

Kheiralla, A., Rahama, O., Saadelnoor, A., Abd-lkareem, D.M. & Nasr, G.M. (2007). Design and Development of a Hydraulic Circuit Bench for Education Purposes. Proceedings of International Conference on Engineering Education–ICEE,

Kulkarni, K.H. & Hinge, G.A. (2020). Experimental study for measuring discharge through compound broad crested weir. *Flow measurement and Instrumentation*, *75*, 101803, doi:10.1016/j.flowmeasinst.2020.101803.

Kumar, A., & Raj, R. (2022). CFD study of flow characteristics and pressure distribution on Re-entrant wing faces of L-shape buildings. *Civil Engineering and Architecture*, *10*(1), 289-304.

Liu, X. & García, M.H. (2008). Three-dimensional numerical model with free water surface and mesh deformation for local sediment scour. *Journal of*

Waterway, Port, Coastal, and Ocean Engineering, *134*(4), 203-217.

Maghrebi, M., Alizadeh, S. & Lotfi, R. (2012). numerical simulation of flow over rectangular broad crested weir (Real case study). The First International Conference on Dams and Hydropower. Tehran, Iran,

Malekzadeh, F., Salmasi, F., Abraham, J. & Arvanaghi, H. (2022). Numerical investigation of the effect of geometric parameters on discharge coefficients for broad-crested weirs with sloped upstream and downstream faces. *Applied Water Science*, *12*(5), 110, https://doi.org/10.1007/s13201-022-01631-5.

Man, C., Zhang, G., Hong, V., Zhou, S. & Feng, Y. (2019). Assessment of turbulence models on bridge-pier scour using Flow-3D. *World Journal of Engineering and Technology*, *7*(2), 241-255.

Mirkhorli, P., Ghaderi, A., Alizadeh Sanami, F., Mohammadi, M., Kuriqi, A. & Kisi, O. (2024). An investigation on hydraulic aspects of rectangular labyrinth pool and weir fishway using FLOW-3D. *Arabian Journal for Science and Engineering*, *49*(4), 6061-6087.

Rady, R. (2011). 2D-3D modeling of flow over sharp-crested weirs. *Journal of Applied Sciences Research*, *7*(12), 2495-2505.

Xu, T. & Jin, Y.-C. (2017). Numerical study of the flow over broad-crested weirs by a mesh-free method. *Journal of Irrigation and Drainage Engineering*, *143*(9), 04017034.

Yakhot, V. & Smith, L.M. (1992). The renormalization group, the ε-expansion and derivation of turbulence models. *Journal of Scientific Computing*, *7*, 35-61.

Zahabi, H., Torabi, M., Alamatian, E., Bahiraei, M. & Goodarzi, M. (2018). Effects of geometry and hydraulic characteristics of shallow reservoirs on sediment entrapment. *Water*, *10*(12), 1725, https://doi.org/10.3390/w10121725.